

RESEARCH ARTICLE

10.1002/2013JB010449

Key Points:

- Petrology-based model of the electrical conductivity of peridotite
- Melt fraction estimate from magnetotelluric data
- Simultaneous interpretation of electrical and seismic data

Supporting Information:

- Readme
- Auxiliary material

Correspondence to:

A. Pommier,
apommier@asu.edu

Citation:

Pommier, A., and E. J. Garnero (2014), Petrology-based modeling of mantle melt electrical conductivity and joint interpretation of electromagnetic and seismic results, *J. Geophys. Res. Solid Earth*, 119, 4001–4016, doi:10.1002/2013JB010449.

Received 17 JUN 2013

Accepted 10 APR 2014

Accepted article online 14 APR 2014

Published online 2 MAY 2014

Petrology-based modeling of mantle melt electrical conductivity and joint interpretation of electromagnetic and seismic results

A. Pommier¹ and E. J. Garnero¹¹School of Earth and Space Exploration, Arizona State University, Tempe, Arizona, USA

Abstract The presence of melt in the Earth's interior depends on the thermal state, bulk chemistry, and dynamics. Therefore, the investigation of the physical and chemical properties of melt is a probe of the planet's structure, dynamics, and potentially evolution. Here we explore melt properties by interpreting geophysical data sets sensitive to the presence of melt (electromagnetic and seismic) with considerations of petrology and, in particular, peridotite partial melting. We present a petrology-based model of the electrical conductivity of fertile and depleted peridotites during partial melting. Seismic and magnetotelluric (MT) studies do not necessarily agree on melt fraction estimates, a possible explanation being the assumptions made about melt chemistry as part of MT data interpretation. Melt fraction estimates from electrical anomalies usually assume a basaltic melt phase, whereas petrological knowledge suggests that the first liquids produced have a different chemistry, and thus a different conductivity. Our results show that melts produced by low-degree peridotite melting (< 15 vol %) are up to 5 times more conductive than basaltic liquids. Such conductive melts significantly affect bulk rock conductivity. Application of our electrical model to magnetotelluric results suggests melt fractions that are in good agreement with seismic estimates. With the aim of a simultaneous interpretation of electrical and seismic data, we combine our electrical results with seismic velocity considerations in a joint model of partial melting. Field electrical and seismic anomalies can be explained by ~1 vol % melt beneath Hawaii and ~1–8 vol % melt beneath the Afar Ridge.

1. Introduction

Melting in response to mantle processes occurs in different geological contexts, such as mid-ocean ridges, oceanic islands, continental rifts, and subduction zones, and depends on the thermal state, bulk chemistry, and dynamics of the Earth's interior. Therefore, the investigation of the physical and chemical properties of melt is a probe of the Earth's structure and dynamics and furthers our understanding of the evolutionary pathways that led to the present-day state of the planet. Because melting influences bulk rock properties, such as seismic velocity and electrical conductivity, partial melting of mantle materials can be modeled using geophysical investigations. Seismic and magnetotelluric (MT) surveys have shown that partially molten regions of high electrical conductivity can generally be correlated with a reduction in seismic velocity [e.g., *Sinha et al.*, 1998; *Naif et al.*, 2013]. However, MT and seismic signals throughout the lithosphere and asthenosphere depend on temperature, chemistry, and geometry (melt interconnection) in differing degrees [e.g., *Schmeling*, 1985, 1986; *Karato*, 1993; *Roberts and Tyburczy*, 1999; *Takei*, 2000; *Faul et al.*, 2004]. If both types of geophysical data can be interpreted in terms of interconnected melt, these interpretations do not necessarily agree on melt fraction estimates, with electrical interpretations usually providing higher melt contents than seismic interpretations (Figure 1). For instance, seismic results in the Hawaiian hot spot region (Figure 1, region 3) are explained by the presence of less than 2 vol % melt [*Laske et al.*, 2011], whereas the interpretation of electromagnetic data suggests the presence of a higher melt fraction, 5–10 vol % [*Constable and Heinson*, 2004]. The interpretation of geophysical data to infer melt fraction requires knowledge of the influence of different parameters (temperature, bulk chemical composition, and geometry) on the measured physical properties [e.g., *Hammond and Humphreys*, 2000a, 2000b; *Pommier*, 2013]. By investigating the effect of these parameters on the rock physical properties, experimental measurements in the laboratory and their modeling are critical as part of geophysical data interpretation.

Possible explanations for the discrepancies in the estimations of melt content from electrical and seismic data can involve the quality of geophysical measurements, as well as assumptions made for the interpretation.

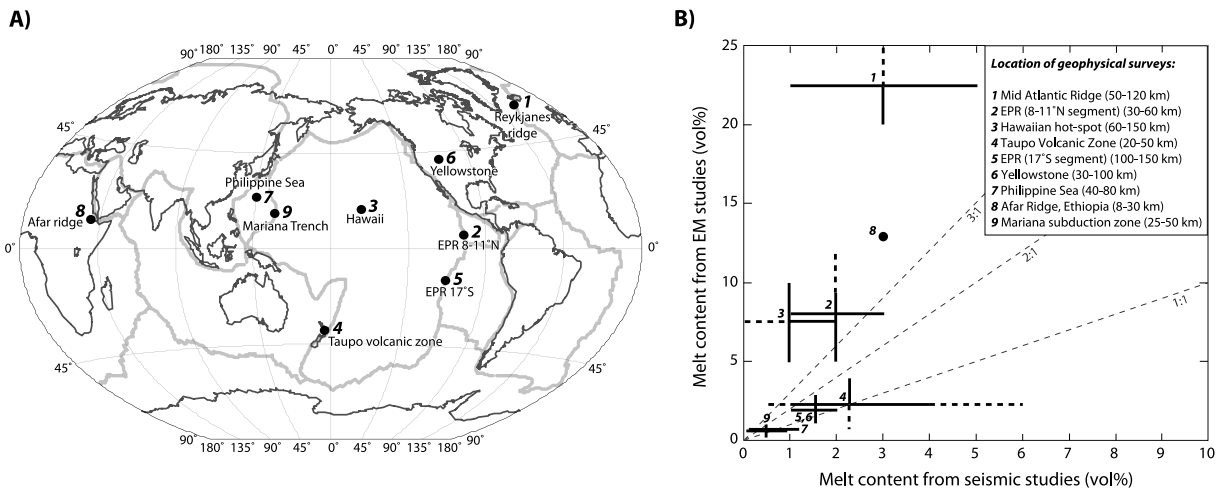


Figure 1. Examples of areas for which both electromagnetic and seismic surveys have been performed. (a) Location. (b) Melt content estimates from both geophysical techniques for the detected anomalies. 1 from *Sinha et al.* [1998] and *Delorey et al.* [2005]; 2 from *Toomey et al.* [2007] and *Key et al.* [2013]; 3 from *Constable and Heinson* [2004] and *Laske et al.* [2011]; 4 from *Heise et al.* [2010] and *Behr et al.* [2010]; 5 from *Toomey et al.* [1998], *Evans et al.* [1999], and *Dunn and Forsyth* [2003]; 6 from *Wagner et al.* [2010] using *Hammond and Humphreys* [2000a] and *Kelbert et al.* [2011]; 7 from *Kawakatsu et al.* [2009] and *Baba et al.* [2010]; 8 from *Desissa et al.* [2013] and *Stork et al.* [2013]; 9 from *Pozgay et al.* [2009] and *Matsuno et al.* [2012].

From a magnetotelluric viewpoint, the choice of laboratory electrical measurements used as part of the interpretation of field results or hypotheses regarding the petrological settings of the investigated area can influence melt fraction estimates. In particular, a significant source of uncertainty on melt fraction estimates from MT studies may lie in the assumptions regarding melt chemistry. Melt fraction from bulk electrical anomalies is usually calculated using mixing models (such as the spheres model [*Hashin and Shtrikman*, 1962] or the tubes model [*Schmeling*, 1986]), with the conductivity of the melt phase taken from laboratory-based conductivity models for synthetic or natural basaltic melts at high temperature [e.g., *Schilling et al.*, 1997; *McGregor et al.*, 1998; *Kelbert et al.*, 2012; *Matsuno et al.*, 2012]. However, this approach does not account for the wide range of chemical compositions through which melt evolves during partial melting under equilibrium or during fractional crystallization [e.g., *Takahashi and Kushiro*, 1983; *Hirschmann et al.*, 1998, 1999]. For instance, a low degree of melting of fertile peridotite (<5%) at 1 GPa produces melts whose bulk chemistry is significantly different from the composition of typical basaltic melts [e.g., *Baker and Stolper*, 1994; *Baker et al.*, 1995]. Because electrical conductivity is sensitive to melt chemical composition [*Roberts and Tyburczy*, 1999; *Gaillard and Iacono Marziano*, 2005; *Pommier et al.*, 2008, 2013], it is expected that the electrical response of molten silicates from low-degree melting should differ from the conductivity of basaltic melt at similar pressure and temperature, hence influencing the estimation of melt fraction. Since isolated pockets of melt do not significantly influence bulk conductivity, the effect of melt composition on bulk conductivity is especially relevant for contexts of interconnected melt, which can occur at very low melt fraction [e.g., *Kohlstedt*, 1992].

In this paper, we explore the effect of melt chemical evolution during peridotite partial melting on electrical conductivity. Partial melting of three chemically distinct peridotites is considered. Based on the existing laboratory database of electrical conductivity of silicate melts, we propose a petrology-based model of the electrical conductivity of peridotite partial melting up to 2 GPa that accounts for the evolution of melt composition along with the extent of melting. Melt conductivities are up to 5 times higher than the conductivity of a basaltic liquid at the same temperature. Depending on the peridotite composition, melt electrical conductivity value at low degree of melting can be higher than 15 S/m, whereas the electrical response of a basaltic melt over the same temperature range does not exceed 8 S/m. Application of our electrical model to MT results allows estimation of melt fraction in hot spot and mid-ocean ridge contexts, and our estimates are in good agreement with melt fractions suggested by seismic studies. Finally, we combine our electrical results with seismic velocity (V_S , V_P) considerations, and apply the resulting joint model of partial melting to the Hawaiian hot spot, the Mid-Atlantic Ridge, and the Afar Ridge.

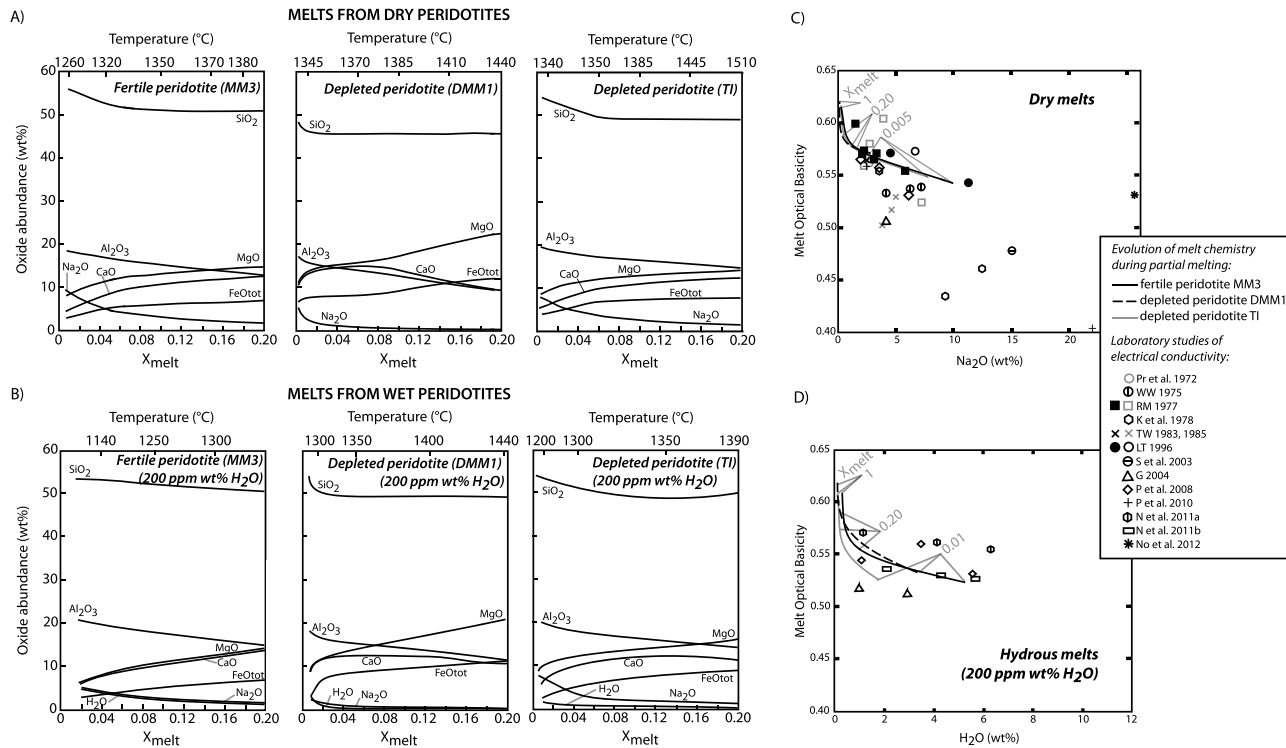


Figure 2. Melt phase chemistry of partially molten fertile and depleted peridotites, $P = 1$ GPa. (a) Variations in oxide contents for fertile (MM3) and two depleted (DMM1 and TI) peridotites for a degree of partial melting up to 20%, using the pMELTS algorithm. Starting compositions from Hirschmann et al. [1998]. Crosses correspond to experimental melts from Walter and Presnall [1994] on a synthetic Iherzolite at 1280°C, 1 GPa; 1310°C, 1.3 GPa; and 1380°C, 1.7 GPa. Circles correspond to experimental melts from Robinson et al. [1998] on the TI composition at 1336°C and 1.5 GPa. (b) Same as Figure 2a with an initial water content of 200 ppm wt % water. (c and d) Comparison between dry (Figure 2c) and hydrous (Figure 2d) melt compositions produced by partial melting and silicate melt compositions investigated as part of electrical conductivity studies in the laboratory. Laboratory studies on dry melts allow modeling of the electrical conductivity of partially molten dry peridotite, while the electrical properties of hydrous melts have been studied for compositions that are not representative of partial melts of hydrous peridotites. Filled symbols correspond to melts whose electrical properties were used to develop our conductivity model. See text for details. Optical Basicity calculated using Pommier et al. [2013]. Pr et al.: Presnall et al. [1972]; WW: Waff and Weill [1975]; RM: Rai and Manghnani [1977]; K et al.: Kawahara et al. [1978]; TW: Tyburczy and Waff [1983, 1985]; LT: Li and Tomozawa [1996]; S et al.: Simonnet et al. [2003]; G: Gaillard [2004]; P et al.: Pommier et al. [2008, 2010]; N et al.: Ni et al. [2011a, 2011b]; No et al.: Noritake et al. [2012].

2. Electrical Conductivity of Peridotites During Partial Melting Processes

2.1. Chemical Considerations

In the Earth's mantle, peridotite melting processes significantly affect the chemical composition of partial melts. For example, because alkalis are incompatible with respect to the minerals in spinel and garnet peridotites, silicate melts produced by small extent of melting of peridotite can contain 6–13 wt % alkalis [e.g., Draper, 1992; Schiano and Clocchiatti, 1994; Baker et al., 1995]. Figures 2a and 2b illustrate variations in liquid composition during equilibrium partial melting at 1 GPa using the pMELTS algorithm [Ghiorso et al., 2002] for partial melting of a fertile (MM3), a depleted (TI), and a very depleted (DMM1) peridotite (bulk rock compositions from Baker and Stolper [1994], Wasylenki et al. [1996], and Robinson et al. [1998], respectively). For calculations with wet peridotite, we considered 200 wt ppm water in the starting composition. All calculations were made at constant oxygen fugacity (Fayalite-Magnetite-Quartz (FMQ) buffer). The sodium-rich content in the first melts produced are in general agreement with experimental results, which supports the validity of our approach that uses pMELTS to compute partial melt compositions. High sodium content has been observed in experimental products of partial melting. In the study by Hirose and Kushiro [1993], liquid compositions from partial melting experiments of spinel Iherzolites at 1 GPa present Na₂O contents up to 4.60 wt %. The results of Walter and Presnall [1994] on a simplified Iherzolite composition showed Na₂O contents in the melt phase ranging of 3.47 and 5.54 at 1 and 1.1 GPa, respectively, and $T < 1280^\circ\text{C}$. At 1.5 GPa, Robinson et al. [1998] measured Na₂O contents of 7.49 wt % in melt from fertile peridotite melting at their

lowest temperature (1267°C), and 4.90 wt % Na₂O in melt from TI peridotite melting at 1315°C. The first melts observed in the experiments by *Wasylenki et al.* [2003] on DMM1 composition present a sodium content of 2.02 wt % at 1275°C and 1 GPa. For a similar melt composition, we note that experimental works observe a lower temperature than the one predicted using pMELTS, particularly for the DMM1 and TI peridotites. In our study, we consider the results from pMELTS, and, because increasing temperature increases electrical conductivity, we assume that the electrical models of the DMM1 and TI peridotites may slightly overestimate the electrical conductivity of partially molten peridotite.

The electrical conductivity of silicate melts depends on its chemical composition and, in particular, strongly increases with alkali content (particularly sodium) and water content [*Bockris et al.*, 1952; *Gaillard*, 2004; *Pommier et al.*, 2008; *Ni et al.*, 2011a, 2011b]. Electrical conductivity is also sensitive to the degree of polymerization of the melt, which can be characterized through its Optical Basicity [e.g., *Moretti*, 2005; *Mathieu et al.*, 2011]. Optical Basicity expresses acid-base interactions within a silicate melt that are determined from Pauling electronegativity [e.g., *Duffy and Ingram*, 1976]. In silicate melts, network modifying cations (e.g., Mg²⁺, Ca²⁺, Fe²⁺, Na⁺, K⁺, and H⁺) are considered as bases (electron donors) and network forming cations (Si⁴⁺ and Al³⁺) as acids (electron receivers). The interested reader is referred to *Pommier et al.* [2013] for details regarding the Optical Basicity calculation for silicate melts and its effect on electrical conductivity.

Figure 2c compares the chemical composition of liquids from partial melting of dry and wet peridotites (from Figures 2a and 2b) to the composition of silicate melts investigated as part of electrical studies in the laboratory. A few laboratory studies also attempted to measure the bulk electrical conductivity of partially molten rocks [e.g., *Roberts and Tyburczy*, 1999; *Partzsch et al.*, 2000; *ten Grotenhuis et al.*, 2005; *Maumus et al.*, 2005]. However, it is not possible to discriminate from these electrical measurements the effect of melt fraction, melt composition, and melt geometry on the bulk conductivity. Therefore, electrical data conductivity studies on partially molten rocks are not considered as part of our modeling.

As shown in Figure 2c, several electrical measurements have been performed on compositions representative of liquids in the 0–20 % melting interval, allowing a conductivity model of peridotite partial melting to be developed. In particular, silicate melts from the studies of *Rai and Manghnani* [1977], *Tyburczy and Waff* [1983], and *Li and Tomozawa* [1996] have sodium content and Optical Basicity close to the dry partial melts considered in our study. The electrical database for hydrous melts is more limited and unavailable for compositions that correspond to the ones of liquids produced from partial melting of hydrous peridotite. Thus, the existing electrical data set for hydrous melts cannot be used to calculate satisfactorily the electrical conductivity of hydrous peridotite during partial melting. As a result, our conductivity model will focus on fertile and depleted dry peridotites, allowing geophysical applications in water-depleted geological contexts for magma genesis, such as hot spots and mid-ocean ridges.

2.2. Petrology-Based Model of the Electrical Conductivity of Partially Molten Peridotites

2.2.1. Electrical Conductivity of the Liquid Phase

We considered the electrical data from the studies of *Rai and Manghnani* [1977], *Tyburczy and Waff* [1983], and *Li and Tomozawa* [1996]. As underlined in Figure 2c, the melt compositions investigated as part of these two studies are representative of the chemistry of liquids for low degrees of partial melting. Therefore, these experimental data are the best candidates to model the evolution of the electrical conductivity of peridotite at low degrees of partial melting. Electrical conductivity results for the mugearite composition from the study by *Rai and Manghnani* [1977] were discarded from our conductivity model (Figure 2, data point in grey), because a long dwell (63 h) at relatively high temperature (950°C) was made during the electrical measurements on this composition, leading probably to significant alkali loss through volatilization and therefore explaining the low conductivity value. For studies that performed measurements at atmospheric pressure, we applied a correction of -0.15 log unit in electrical conductivity to account for the effect of a pressure of 1 GPa, in agreement with the effect of pressure observed in experimental studies [e.g., *Tyburczy and Waff*, 1983]. The temperatures considered in the experiments of *Rai and Manghnani* [1977] (500–1500°C) cover the temperature range of peridotite partial melting up to 20 vol % (~1250–1400°C for the fertile peridotite and ~1340–1510°C for the depleted peridotites; see Figures 2a and 2b), while *Li and Tomozawa* [1996] conducted experiments from 950 to 1250°C. Their melt compositions correspond to the composition of the partial melts that are produced at temperatures from 1300 to 1370°C, and, as a result, we extrapolated their conductivity model to these higher temperatures of interest.

The evolution of melt electrical conductivity during partial melting (i.e., as a function of melt fraction and temperature) at 1 GPa is shown in Figure 3a. For the three peridotites, low-degree partial melting produces conductive melts (>7 S/m). The first melts produced are silicate liquids whose conductivities are up to 5 times higher than the conductivity of a basaltic melt at the same temperature. This is essentially explained by the very high Na_2O contents of these liquids (Figure 2a). For the three peridotites, the observed decrease in conductivity along with an increase in temperature suggests that electrical conductivity of these liquids is controlled by melt chemistry rather than by temperature. We propose the following empirical equations to model the electrical conductivity of melt produced from peridotite partial melting. These equations represent the best fit to the considered data set (Figure 3a). In the case of MM3 peridotite, for a melt content X : $0.1 \leq X \leq 15$ vol %,

$$\sigma_{\text{melt}} = 205.36X^2 - 95.414X + 19.717 \quad (1)$$

For DMM1 peridotite, for $0.1 \leq X \leq 10$ vol %

$$\sigma_{\text{melt}} = -5807.1X^3 + 1495.2X^2 - 105.29X + 10.045 \quad (2)$$

For TI peridotite, for $0.1 \leq X \leq 15$ vol %

$$\sigma_{\text{melt}} = -2496.1X^3 + 1320.1X^2 - 231.76X + 21.449 \quad (3)$$

with σ_{melt} in S/m and X in vol %. Equations (1) to (3) reproduce considered laboratory conductivity data (Figure 3a) with a correlation coefficient of 0.993, 0.981, and 0.988, respectively, and an average error of ± 0.2 for MM3 peridotite, ± 0.1 for DMM1 peridotite, and ± 0.4 for TI peridotite.

For all three peridotites, higher degrees of partial melting produce melts with low sodium contents and high Optical Basicity (Figure 2c). As shown in Figure 2c, one silicate melt in particular is representative of these compositions and comes from the study of *Rai and Manghnani* [1977] (Optical Basicity of 0.60 and sodium content of 1.48 wt % Na_2O). The electrical response of this basaltic melt can be used to model the electrical conductivity of liquids produced at high degrees of partial melting ($X > 15$ vol % for MM3 and TI peridotites, and $X > 10$ vol % for DMM1 peridotite) (Figure 3a). The experimental data from *Rai and Manghnani* [1977] show that the electrical conductivity of this basaltic melt can be modeled using the following Arrhenian equation:

$$\sigma_{\text{melt}} = 2.321 \times 10^5 \exp\left(\frac{-1.40 \times 10^5}{RT}\right) \quad (4)$$

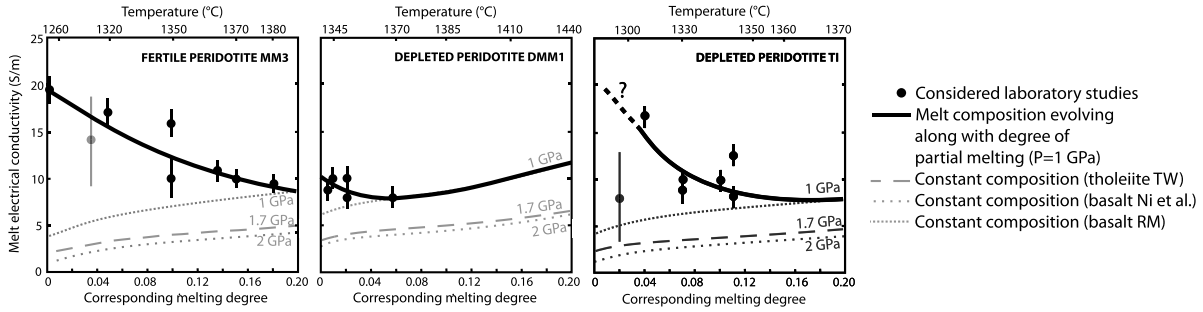
with σ_{melt} the electrical conductivity of melt (S/m), T the temperature (K), and R the universal gas constant ($8.314 \text{ J mol}^{-1} \text{ K}^{-1}$). Equation (4) accounts for the correction of pressure effect at 1 GPa. As shown in Figure 3a, liquids produced at high degrees of partial melting present an increase in electrical conductivity with temperature. This suggests that the high temperatures ($>1400^\circ\text{C}$) govern the electrical conductivity regime for these liquids. For the three peridotites, changes in the chemistry of liquids coming from high-degree partial melting are less dramatic than during the first steps of the melting process, which diminishes the effect of melt chemistry on electrical conductivity.

At a first approximation, our melt conductivity model can be used at a pressure of 2 GPa by applying the following correction to equations (1) to (4):

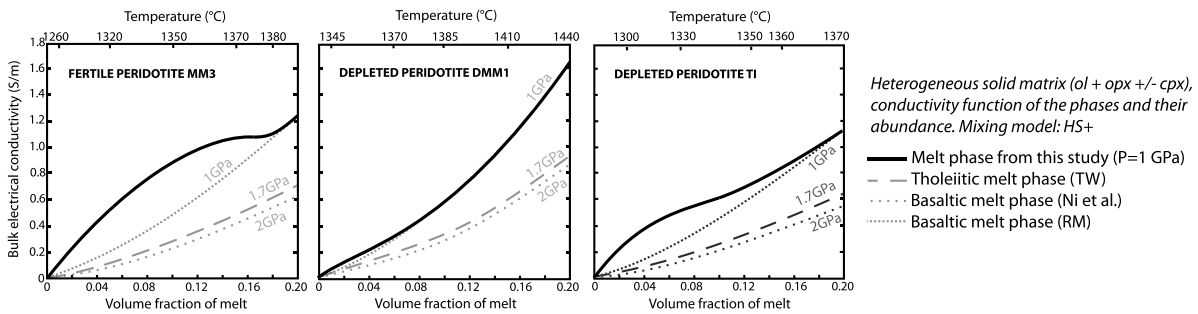
$$\log(\sigma_{\text{melt}})|_{2\text{GPa}} = \log(\sigma_{\text{melt}})|_{1\text{GPa}} - 0.2 \quad (5)$$

A higher temperature (160°C (± 20) higher) is needed at 2 GPa to produce the same melt fraction: for instance, a temperature of 1270°C at 1 GPa produces 1 vol % of melt from the MM3 peridotite, while a similar melt fraction is obtained for a temperature of $\sim 1430^\circ\text{C}$ at 2 GPa. According to the experimental data of *Ni et al.* [2011a], such an increase in temperature increases the conductivity of melt by ~ 0.55 log units (± 0.05). The effect of temperature is partially counterbalanced by (1) the effect of pressure, for an increase of 1 GPa decreases melt conductivity by ~ -0.15 log unit (± 0.05) [*Tyburczy and Waff*, 1983] and (2) the effect of melt composition, because melts at 2 GPa have a lower sodium content than at 1 GPa (for a similar degree of partial melting) and are therefore less conductive. For instance, pMELTS calculations show that low-degree melting of MM3 peridotite ($X \sim 0.01$) produces liquids with a Na_2O content of 8.2 wt % at 1 GPa and 7.6 wt % at 2 GPa. Experiments performed by *Walter and Presnall* [1994] at 1–1.1 GPa and 2 GPa showed Na_2O contents in the

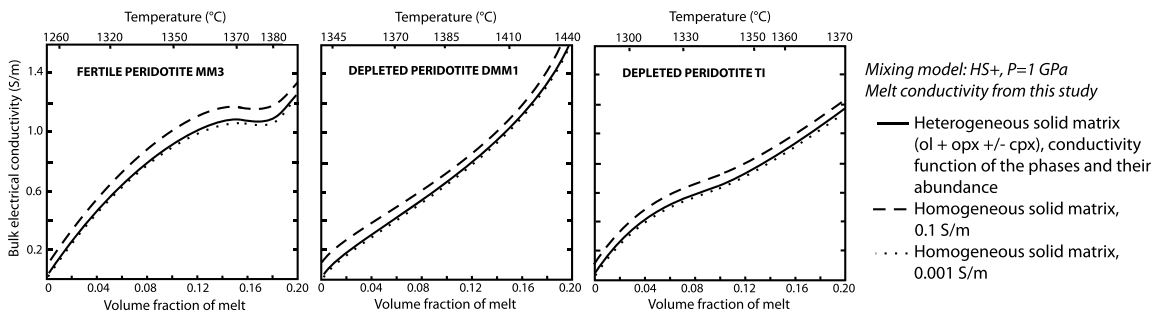
A) MELT CONDUCTIVITY



B) BULK CONDUCTIVITY: EFFECT OF MELT COMPOSITION



C) BULK CONDUCTIVITY: EFFECT OF SOLID MATRIX COMPOSITION



D) BULK CONDUCTIVITY: EFFECT OF GEOMETRY

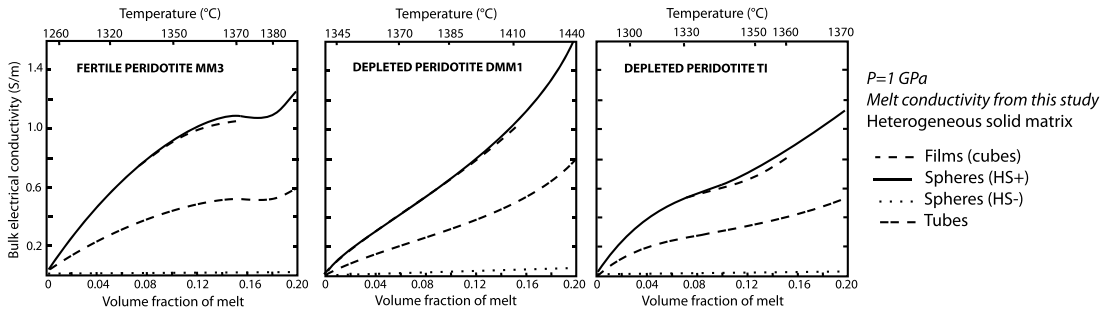


Figure 3. Electrical conductivity model for partially molten fertile (MM3) and depleted (DMM1) peridotites up to 20 vol % of melt. Indicated temperatures are for melting at 1 GPa. (a) Melt electrical conductivity from partial melting of peridotite. Melt chemistry at defined T and volume fraction calculated using MELTS calculations. Data points are from laboratory studies selected from Figure 2c. Dashed lines are melt conductivities for basaltic melts and tholeiitic melt with constant chemistry (from *Rai and Manghnani* [1977] (RM), *Tyburczy and Waff* [1983] (TW), and *Ni et al.* [2011a] (Ni et al.), respectively). Data from RM (at 1 bar) were calculated for a pressure of 1 GPa using the pressure correction detailed in the text. (b) Bulk electrical conductivity using the Hashin-Shtrikman upper bound (HS+) and a solid matrix conductivity based on the nature and proportion of mineral phases (olivine (ol), orthopyroxene (opx), and clinopyroxene (cpx)). See text for details. Melt phase conductivity from our model (equations (1) to (3)). (c) Bulk electrical conductivity using the HS+ bound. Liquid phase conductivity is from our model. Solid phase conductivity of 0.1 S/m, 0.001 S/m, and based on the nature and proportion of mineral phases. (d) Bulk electrical conductivity considering a solid phase conductivity function of the nature and proportion of minerals and a liquid phase conductivity from our model. Upper bound conductivities are for the film model [Waff, 1974], HS+ (spheres, liquid matrix) bound [Hashin and Shtrikman, 1962], and the tube model [Grant and West, 1965]. Lower bound conductivities are calculated using the HS lower bound (spheres, solid matrix) [Hashin and Shtrikman, 1962].

melt phase of 3.47–5.54 wt % and 4.96–1.15 wt %, respectively. Their results are consistent with a small decrease in sodium content when pressure increases from 1 to 2 GPa. In the experiments by *Blundy et al.* [1995], the melt phase contains 4 wt % Na₂O at 1 GPa and 1390°C, and 6 wt % at 1500°C and 2 GPa (runs 93PC11 and 93PC20), which does not suggest a strong depletion in sodium at comparable degrees of melting. According to electrical laboratory studies [*Rai and Manghnani, 1977; Pommier et al., 2008*], such a change in melt chemistry when increasing pressure is likely to account for a change in conductivity of ~ -0.10 to -0.20 log unit. As a consequence, for a defined melt fraction, the change in melt conductivity from 1 to 2 GPa is estimated to be about 0.20 log unit in the 0–20% melting interval and 0.15 log unit at higher extent of melting.

We assume that pMELTS calculations reproduce experimental results rather satisfactorily over the P range 1–2 GPa and can be used to model mantle partial melting. However, over a larger amplitude pressure range, studies of sodium partition coefficient between melt and clinopyroxene have demonstrated that sodium preferentially goes to the solid phase at high pressure [*Blundy et al., 1998; Robinson et al., 1998*], leading to a significant decrease in the sodium content of the melt phase with increasing pressure, and thus decreasing the electrical conductivity of the melt phase substantially. Therefore, we do not recommend the use of our conductivity model developed at 1 GPa at pressure higher than 2 GPa.

2.2.2. Electrical Conductivity of the Solid Phase

For each temperature of partial melting process, calculations using the MELTS algorithm provide with the composition and abundance of minerals that are expected to be in equilibrium with the melt phase. For both kinds of peridotites, these minerals are olivine, orthopyroxene, spinel, and sometimes clinopyroxene. With proportions less than 5 vol %, spinel is considered as a minor phase that, therefore, does not contribute significantly to the bulk conductivity. As a result, we calculated the electrical conductivity of the solid matrix based on an assemblage of olivine and pyroxenes.

Olivine conductivity was determined using the SOE3 model at the FMQ redox buffer [*Constable, 2006*], and the electrical conductivity of pyroxenes was calculated using the laboratory-based models by *Dai and Karato* [2009] and *Yang et al.* [2011], for orthopyroxene and clinopyroxene, respectively. Because the effect of pressure from 1 to 2 GPa is negligible on the electrical conductivity of these minerals, our calculations of the electrical conductivity of the solid matrix are valid at 1 and 2 GPa. For each temperature of the partial melting process, the conductivity of the solid matrix $\sigma_{\text{solid matrix}}$ is calculated using the geometric means [*Shankland and Duba, 1990*]

$$\sigma_{\text{solid matrix}} = \prod_i (\sigma_i^{x_i}) \quad (6)$$

with σ_i the conductivity of phase i (S/m) and x_i its volume fraction. The electrical conductivity of the solid matrix for a degree of partial melting up to 20 vol % at 1 GPa ranges from 9.10^{-3} to 0.02 S/m for the MM3 peridotite, from $\sim 2.6.10^{-3}$ to 0.02 for the DMM1 peridotite, and from 0.02 to 0.05 for the TI peridotite (see supporting information).

2.2.3. Bulk Electrical Conductivity

Calculations of bulk electrical conductivity (i.e., liquid and solid phases) are presented in Figures 3b–3c. Conductivity values are listed in the supporting information. The effect of chemical changes in melt composition on bulk conductivity is observed for all peridotites and is particularly significant for the MM3 and TI peridotites (Figure 3b). For 8.5 vol % of partial melting, the electrical conductivity of the partially molten MM3 peridotite is ~ 0.8 S/m, i.e., more than 2 times higher than the conductivity of an assemblage that considers a basaltic melt as the liquid phase (0.35 S/m). Five vol % of partial melting of the TI peridotite is characterized by an electrical conductivity of ~ 0.43 S/m, which is also more than 2 times higher than the conductivity of an assemblage that considers a basaltic melt (0.20 S/m). In contrast, only the liquids produced during the first ~ 2 vol % of partial melting of the DMM1 peridotite are very conductive (> 8 S/m, Figure 3a), and these amounts of melt are too low to affect dramatically the bulk electrical conductivity (Figure 3b).

As shown in Figure 3c, the effect of the solid matrix conductivity on bulk conductivity is negligible at our conditions and for an interconnected melt phase (Hashin-Shtrikman upper bound) [*Hashin and Shtrikman, 1962*]. Accounting for each mineral phase or assuming a homogenous conductivity value for the solid matrix does not lead to significant discrepancies. The effect of geometry of the liquid and solid assemblage on bulk

conductivity is more important than the solid matrix composition. Several two-phase mixing models have been proposed, and in Figure 3d, we consider the following geometrical configurations:

1. The cubes model, where thin films of melt of uniform thickness surround cubic grains (for melt fractions less than approximately 15% and continuous grain boundary wetting) [Waff, 1974]

$$\sigma_{\text{bulk}} = \left[1 - (1 - X_{\text{melt}})^{2/3} \right] \sigma_{\text{melt}} \quad (7)$$

2. The spheres model, consisting of spheres of solid (or melt) isolated from each other in a liquid (or solid) matrix, called Hashin-Shtrikman upper (lower) bound [Hashin and Shtrikman, 1962]

$$\sigma_{\text{bulk}}|_{\text{HS}+} = \sigma_{\text{melt}} + \frac{1 - X_{\text{melt}}}{\left(\frac{1}{\sigma_{\text{solid}} - \sigma_{\text{melt}}} \right) + \left(\frac{X_{\text{melt}}}{3\sigma_{\text{melt}}} \right)} \quad (8)$$

$$\sigma_{\text{bulk}}|_{\text{HS}-} = \sigma_{\text{solid}} + \frac{X_{\text{melt}}}{\left(\frac{1}{\sigma_{\text{melt}} - \sigma_{\text{solid}}} \right) + \left(\frac{1 - X_{\text{melt}}}{3\sigma_{\text{solid}}} \right)} \quad (9)$$

3. The tubes model [Schmeling, 1986], in which the melt is distributed in equally spaced tubes:

$$\sigma_{\text{bulk}} = \frac{1}{3} X_{\text{melt}} \sigma_{\text{melt}} + (1 - X_{\text{melt}}) \sigma_{\text{solid}} \quad (10)$$

In each case, X_{melt} is the melt fraction, σ_{bulk} is the bulk electrical conductivity, σ_{melt} is the electrical conductivity of the melt phase, and σ_{solid} is the electrical conductivity of the solid phase (all conductivities are in S/m).

The Hashin-Shtrikman upper bounds, the films model, and the tubes model provide estimates for a well-interconnected melt phase. The tubes model gives a higher melt fraction for a given electrical conductivity value, and hence represents the upper bound of melt fraction determination from electrical conductivity. If the tube geometry is relevant in some high deformation contexts where electrical anisotropy is observed [e.g., Caricchi et al., 2011; Naif et al., 2013], the Hashin-Shtrikman bounds are considered the narrowest upper and lower bounds in the absence of knowledge of the geometrical arrangement of the constituent phases [Hashin and Shtrikman, 1962; Berryman, 1995]. Thus, we will consider this mixing model as part of geophysical applications.

3. Geophysical Implications

3.1. Melt Fraction Estimates in the Upper Mantle Using MT Data

The geological processes involving silicate melts probed using MT soundings are usually explained by melt fractions <20%, which highlights the need for electrical models as the one proposed in this study. For instance, the suboceanic upper mantle partially melts between ~5 and 20% to produce mid-ocean ridge basalt (MORB) during near-adiabatic upwelling [e.g., Klein and Langmuir, 1987; McKenzie and Bickle, 1988; Bonatti et al., 2003], and MT studies are successfully used to detect these partially molten zones below mid-ocean ridges [e.g., Sinha et al., 1998; Evans et al., 1999; Baba et al., 2006; Key et al., 2013].

Our conductivity model shows that the effect of melt chemistry on the bulk electrical conductivity of partially molten peridotites MM3 and T1 is significant for a degree of melting up to ~10–15 vol %, whereas it will not affect significantly the bulk conductivity of peridotite DMM1 (Figure 3b). A partially molten peridotite with a composition close to the one of MM3 or T1 is more conductive than an assemblage assuming a basaltic composition as the liquid phase. As a consequence, our conductivity model also suggests that the melt fraction needed to explain a field electrical anomaly will be lower than a melt fraction estimate involving a liquid composition that is not based on petrological considerations.

Melt fraction estimates using equations (1) to (4) are presented in Table 1 and Figure 4 for the different locations shown in Figure 1 (except the context of the Mariana Arc, since melts in this subduction context are

Table 1. Melt Fractions Estimates Required to Explain Seismic and Electromagnetic Data in Water-Depleted Peridotite Partial Melting Contexts^a

Location	Approximate Depth of the Anomaly (km)	Conductivity of the Anomaly (S/m)	Fraction Estimates	Peridotite Used for Melt	Melt Fraction (vol %) ^b	Melt Fraction (vol %) From Seismic Studies	References
1. Mid-Atlantic Ridge (Reykjanes Ridge)	50–120	0.05–0.17	Depleted	Depleted	0.3–2.5	A few vol %	Delorey <i>et al.</i> [2005]; Sinha <i>et al.</i> [1998]
2. East Pacific Rise (8–11°N segment)	30–60	0.1–1	Depleted	Depleted	1.6–15	1–3	Toomey <i>et al.</i> [2007]; Key <i>et al.</i> [2013]
3. Hawaiian hot spot	60–150	0.03–0.10	Fertile	Fertile	1 or less	<2	Laske <i>et al.</i> [2011]; Constable and Heinson [2004]
4. Taupo Volcanic Zone	20–50	0.1–1	Fertile	Fertile	0.8–5	<6	Stratford and Stern [2006]; Heise <i>et al.</i> [2010]
5. East Pacific Rise (17°S segment)	100–150	0.01–0.3	Depleted	Depleted	<5	1–2	Toomey <i>et al.</i> [1998]; Dunn and Forsyth [2003]; Evans <i>et al.</i> [1999]
6. Yellowstone hot spot	30–100	0.05–1	Fertile	Fertile	0.5–5	1–2	Smith <i>et al.</i> [2009] using Hammond and Humphreys [2000a], Kelbert <i>et al.</i> [2011]
7. Philippine Sea	40–80	<0.04	Depleted and Fertile	Depleted and Fertile	0.2–0.5	0.5	Kawakatsu <i>et al.</i> [2009]; Baba <i>et al.</i> [2010]
8. Afar Ridge, Ethiopia	8–30	0.15–0.65	Depleted	Depleted	3–13	3	Desissa <i>et al.</i> [2013]; Stork <i>et al.</i> [2013]

^aMelt fractions from our model are calculated using equations (1) to (5).

^bAt a depth corresponding to the top of the geophysical anomaly (1 or 2 GPa).

volatile rich [e.g., Kelley *et al.*, 2010]). There is a general good agreement with melt content estimates from seismic studies in the same locations (hot spots and mid-ocean ridges). One exception regards the East Pacific Rise (8–11°N segment), for which the melt content estimate from electrical data is significantly higher than the one suggested from seismic data (up to 15 vol % versus 1–3 vol %). As suggested by Key *et al.* [2013], it is possible that this detected geophysical anomaly contains hydrous and carbonated fluids that would noticeably increase the conductivity of liquids produced from peridotite partial melting. In such a scenario, our dry melting conductivity model would not be suitable for estimating a melt fraction.

Our model has been developed for partial melting of chemically distinct peridotites under equilibrium conditions. Therefore, it aims to approximate batch melting rather than to predict the electrical conductivity of melt undergoing fractional crystallization, in which case melt begins separating from the solid residue once interconnected [e.g., McKenzie, 1984]. Fractional crystallization experiments by Falloon *et al.* [2008] on the MM3 peridotite composition at 1 and 1.5 GPa show that a low degree of melting will produce liquids that are less enriched in sodium than under equilibrium conditions (Na₂O from 3 to 5 wt % versus 3 to ~9 wt %, respectively). In terms of electrical properties, these findings suggest that the electrical conductivity of liquids from fractional crystallization is lower (possibly a few tenths of log unit) than the electrical conductivity under equilibrium conditions. Therefore, the electrical conductivity of melts undergoing fractional crystallization processes is likely to range between conductivity values from our equilibrium model and conductivity of basaltic melts (Figure 3a).

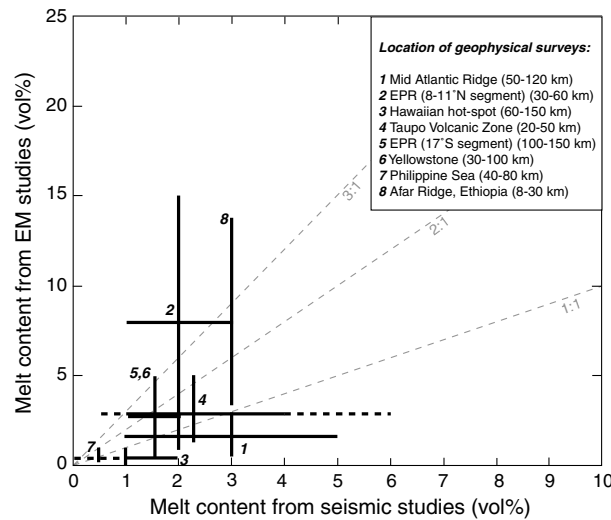


Figure 4. Melt content estimates from electromagnetic and seismic studies in the same locations as in Figure 1b, after correction of electrical melt fraction estimates using our model (equations (1) to (5)).

Actually, MORBs are considered to represent the final product of these melts that have evolved primarily through fractional crystallization as a result of cooling at shallow levels [e.g., Sinton and Detrick, 1992].

3.2. Electrical Conductivity-Seismic Velocity Model of Partially Molten Peridotites

Owing to the general good agreement between melt fraction estimates from our electrical modeling and seismic studies (Table 1), we propose to further the comparison between electrical conductivity and seismic velocity of peridotite partial melting. Schmeling [1986] compared electrical conductivities to elastic and anelastic properties for different idealized geometries, melt distributions, and melt fractions. However, petrological constraints, such as melt chemical evolution during partial melting or the dependence of temperature and melt fraction to geophysical properties, were not considered as part of these previous numerical models. Our seismic and electrical comparison considers two configurations involving an isotropic melt geometry (i.e., in one case, melt is interconnected (liquid matrix), and in the other case, melt is under the form of isolated pockets (solid matrix)).

Our conductivity-velocity comparison is based on the respective dependence of electrical conductivity and seismic velocity (shear and compressional, and V_S and V_P , respectively) to melt fraction and is illustrated in Figures 5 and 6. The relationship between electrical conductivity and melt fraction corresponds to the model presented in this study, where the liquid phase conductivity is calculated using equations (1) to (3) for low melt fractions, equation (4) for high melt fractions, and equation (5) for calculations at 2 GPa. The electrical conductivity of the solid matrix accounts for the nature and proportions of the mineral phases at each temperature and is calculated using equation (6). We considered the Hashin-Shtrikman bounds (equations (8) and (9)) to calculate bulk electrical conductivities.

The relationship between seismic velocities (V_S and V_P) and melt fraction corresponds to the modeling study by Mainprice [1997], which calculates velocities considering different models for effective isotropic media. One model, called the Gassmann model [Gassmann, 1951], is particularly appropriate since it models the low-frequency domain of marine seismic field experiments (from 1 to a few tens of Hz). By combining Gassmann's work with higher-frequency velocity models (the differential effective medium model [Boucher, 1976] and the self-consistent scheme model [Berryman and Berge, 1993]), Mainprice [1997] also proposed a means of determining the high-frequency velocity and hence attenuation. Therefore, we used the Gassmann model modified by Mainprice [1997] to estimate V_S and V_P values as a function of melt fraction.

The shape of the melt inclusions and, in particular, the aspect ratio, influences significantly seismic wave velocities [e.g., Faul et al., 2004]. The Hashin-Shtrikman bounds used in our study consider spherical melt inclusions. Theoretical modeling showed that the effect of partial melt on V_S and V_P using this geometry is

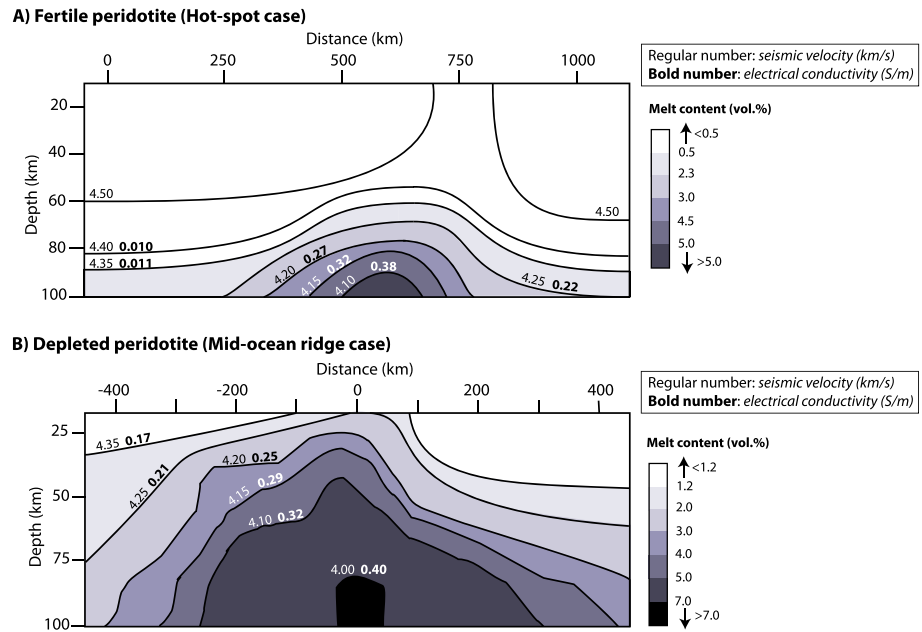


Figure 5. Conductivity-shear wave velocity comparison for (a) a hot spot context and (b) a mid-ocean ridge context. Numbers are V_S values (km/s), and bold numbers are electrical conductivity values (S/m). Velocity lines are from seismic profiles from *Laske et al.* [2011] for the Hawaiian hot spot and *Delorey et al.* [2005] for the Mid-Atlantic Ridge. Melt content estimates are obtained using the model by *Mainprice* [1997] and electrical conductivity values from our model for MM3 and T1 peridotites (equations (1) and (3) to (5)). Position of the ridge in Figure 5b corresponds to distance 0 km. See text for details.

similar to the one that considers melt tubules [*Watt et al.*, 1976; *Williams and Garnero*, 1996], implying that our model can be used to model environment with tubular melt inclusions. Actually, for melt fractions up to 0.4, differences in seismic velocities between these two geometries are less than 0.05 on V_S reduction and less than 0.02 on V_P reduction. The same studies suggest that our model can also predict V_S and V_P values for melt film geometry (aspect ratio of 0.05) with a difference in V_S and V_P reduction less than 0.10 and 0.05, respectively. Melt films with an aspect ratio of 0.01 will not be reproduced satisfactorily with our model. Melt tubule geometry can be particularly relevant in contexts where melt alignment is expected (such as mid-ocean ridges), leading to seismic and electrical anisotropy [*Kawakatsu et al.*, 2009; *Caricchi et al.*, 2011]. The lower and upper bounds of our conductivity-velocity model (Figure 6) provides an estimate of both electrical and seismic anisotropy.

In the study by *Mainprice* [1997], seismic velocities are estimated for a liquid-solid assemblage made of basaltic melt and peridotite (harzburgite) at 1200°C and 0.2 GPa. We accounted for the effect of temperature on seismic velocities using, as a first approximation, the following empirical equations [*Stacey*, 1992]:

$$\left. \frac{d \ln(V_s)}{dT} \right|_p = -5 \times 10^{-5} \text{K}^{-1} \quad (11)$$

and

$$\left. \frac{d \ln(V_p)}{dT} \right|_p = -2.5 \times 10^{-5} \text{K}^{-1} \quad (12)$$

However, for both peridotites, the effect of temperature on V_S and V_P values is negligible on the investigated T range, in agreement with previous estimates of T dependence of seismic velocities in the Earth's mantle [e.g., *Duffy and Anderson*, 1989; *Stacey*, 1992]. We assume that seismic velocities are less sensitive than electrical conductivity to melt chemistry, and therefore, that the chemical changes in melt chemistry considered in our study do not significantly affect seismic velocities. *Mainprice* [1997] also underlined that the effect of pressure on seismic velocities can be ignored, estimated to be only 0.15 km/s from 1 to 2 GPa.

The dependence of seismic velocity and electrical conductivity on melt fraction is illustrated in Figure 5 for two typical contexts: a hot spot, as an example of fertile peridotite melting, and a mid-ocean ridge, as an

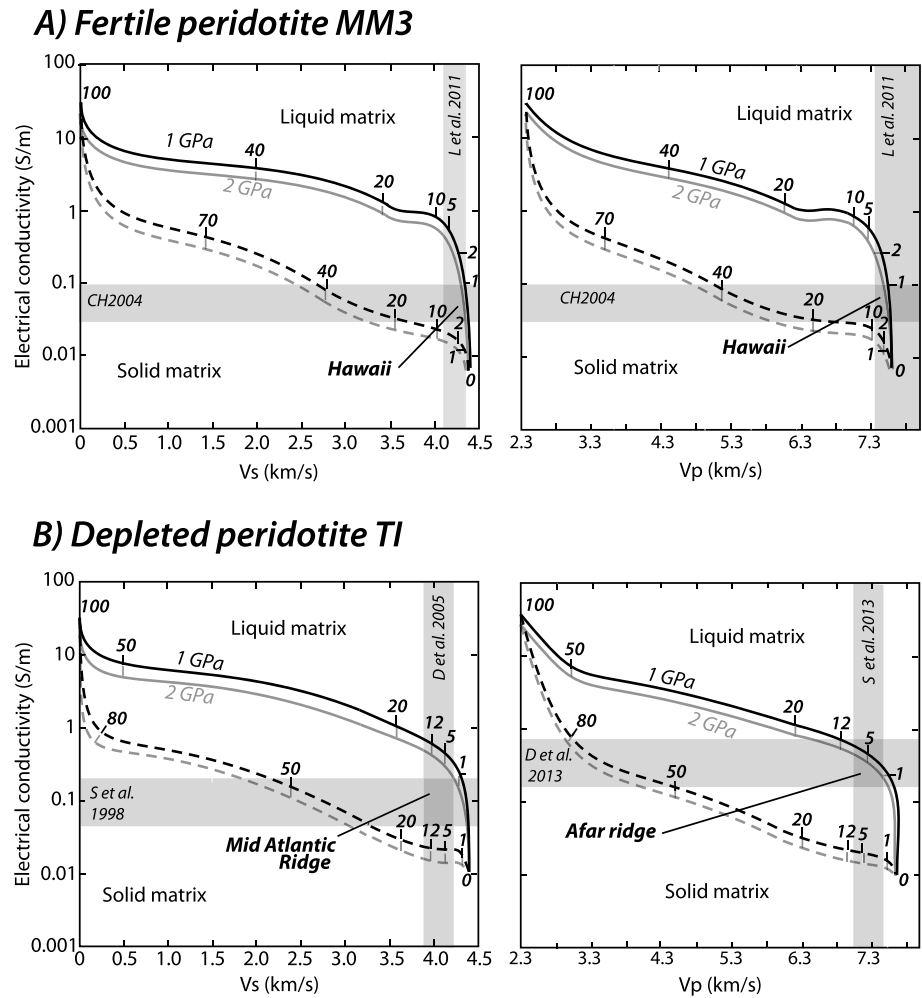


Figure 6. Comparison between electrical conductivity and seismic velocities (V_S and V_P) during peridotite partial melting at 1 and 2 GPa. Numbers in italic are vol % of melt. Electrical conductivities are calculated using our petrology-based model (equations (1) to (4) for melt conductivity, equation (5) for solid matrix conductivity, and equations (8) (upper bound, full line) and (9) (lower bound, dashed line) for bulk conductivity). Seismic parameters computed after the model by Mainprice [1997]. See text for details. (a) Model for fertile peridotite. Comparison with field data from the Hawaiian hot spot [Constable and Heinson, 2004; Laske et al., 2011]. (b) Model for depleted peridotite. Comparison with field data from the Mid-Atlantic Ridge [Sinha et al., 1998; Delorey et al., 2005].

example of depleted peridotite melting. Contoured shear wave velocities come from Laske et al. [2011] (for the hot spot case) and Delorey et al. [2005] (for the mid-ocean ridge case). Using modeling results from Mainprice [1997], we interpreted V_S values in terms of melt fraction and calculated electrical conductivity values corresponding to the variable shear wave velocities using equations (1) to (5). The two synthetic models in Figure 5 underline that, for similar shear wave velocity (and thus, melt fraction), predicted electrical conductivities in the hot spot context are in the same range as the ones under the mid-ocean ridge. This is explained by the small chemical differences in major oxide content between MM3 and T1 peridotite partial melting (Figure 2), leading to comparable bulk electrical conductivities. For instance, the presence of ~3 vol % melt that corresponds to a V_S value of 4.20 km/s is characterized by a bulk electrical conductivity value of 0.26 (± 0.01) S/m in both hot spot and mid-ocean ridge contexts. In Figures 5a and 5b, the outline of the geophysical anomalies presents electrical conductivity values that are in general agreement with the bulk electrical conductivity of anomalies detected in magnetotelluric studies (~0.10 S/m in Hawaii [Constable and Heinson, 2004]; ~0.17 S/m under the Mid-Atlantic Ridge [Sinha et al., 1998]). The core of the anomalies is slightly more conductive than observed in field (>0.40 S/m in both cases).

A direct means of conversion of electrical conductivity values into V_S or V_P values as a function of melt fraction is presented in Figure 6 for peridotites MM3 and TI. Comparison with field data considers the Hawaiian hot spot [Constable and Heinson, 2004; Laske et al., 2011], the Mid-Atlantic Ridge (Reykjanes Ridge) [Sinha et al., 1998; Delorey et al., 2005], and the Afar Ridge [Desissa et al., 2013; Stork et al., 2013]. The combination of field conductivity data and seismic velocities defines an intersection area in the plot space of electrical conductivity versus seismic velocity (V_S or V_P). This area favors a mutually consistent interpretation of the considered data pair in terms of geometry (defined by the location of the intersection area compared to the position of the liquid matrix curve and the solid matrix curve), melt fraction, and hence temperature. The geophysical anomaly detected below the Hawaiian hot spot (>60 km depth) is compatible with the presence of well interconnected ~1 vol % melt or less (Figure 6a). Seismic data in the Mid-Atlantic Ridge are compatible with a melt content ranging from ~2 to 12 vol %; however, the incorporation of MT results favors the lowest estimates, narrowing this range to ~0.30–3.0 vol % (Figure 6b, left). In the case of the Afar Ridge (Figure 6b, right), melt fraction estimates from our electrical conductivity model are in very good agreement with estimates from Desissa et al. [2013] (up to 13 vol %), and the superimposition of the seismic results from Stork et al. [2013] allows narrowing the estimate (1 to 8 vol % melt). The joint data approach helps narrow the uncertainty range of melt fraction possibilities that would be estimated from only one geophysical technique, illustrating the fact that both geophysical techniques benefit from each other's information.

Our model is based on idealized melt geometries. However, these geometries are able to reproduce rather satisfactorily electrical conductivities measured experimentally on melt-bearing aggregates [e.g., ten Grotenhuis et al., 2005; Caricchi et al., 2011]. Also, in some cases, unexplored conduction or relaxation mechanisms, or geometry effects, may dominate over the approach presented in this paper, and further electrical studies in the laboratory are needed to quantify their effects on bulk electrical conductivity. If Figures 5 and 6 should be regarded as relatively rough estimates, a systematic application of our model provides a comprehensive insight into the electrical behavior of a partial melt, as a function of composition, temperature, and melt fraction, and improves the comparison between magnetotelluric and seismic results.

4. Concluding Remarks

We have developed a petrology-based conductivity model of the electrical conductivity of partial melting of three chemically distinct peridotites valid at pressures up to 2 GPa. Particular attention was given to the 0–20% melting interval, where dramatic changes in melt chemistry can control bulk electrical conductivity. Our results highlight the importance of estimating melt fractions in the upper mantle from magnetotelluric surveys by accounting for melts compositions that are in agreement with petrological knowledge. We show that the electrical conductivity of low-degree partial melting of a peridotite can be significantly underestimated if the liquid phase is assumed to be basaltic, resulting in overestimated melt fractions from bulk conductivity values.

Melt estimates using our model in hot spot and mid-ocean ridge contexts are in good agreement with estimates from seismic studies. In an attempt to promote joint geophysical interpretations, we propose a model relating electrical conductivity to seismic velocities V_S and V_P as a function of melt fraction during peridotite partial melting.

Acknowledgments

The authors thank M. Hirschmann for fruitful discussions as well as a constructive review and an anonymous reviewer for helpful comments. A.P. acknowledges financial support from the SESE Exploration Postdoctoral Fellowship.

References

- Baba, K., A. D. Chave, R. L. Evans, G. Hirth, and R. L. Mackie (2006), Mantle dynamics beneath the East Pacific Rise at 17 degrees S: Insights from the Mantle Electromagnetic and Tomography (MELT) experiment, *J. Geophys. Res.*, *111*, B02101, doi:10.1029/2004JB003598.
- Baba, K., H. Utada, T.-N. Gotob, T. Kasayac, H. Shimizua, and N. Tada (2010), Electrical conductivity imaging of the Philippine Sea upper mantle using seafloor magnetotelluric data, *Phys. Earth Planet. Int.*, *183*, 44–62, doi:10.1016/j.pepi.2010.09.010.
- Baker, M. B., and E. M. Stolper (1994), Determining the composition of high-pressure mantle melts using diamond aggregates, *Geochim. Cosmochim. Acta*, *58*, 2811–2827.
- Baker, M. B., M. M. Hirschmann, M. S. Ghiorso, and E. M. Stolper (1995), Compositions of near-solidus peridotite melts from experiments and thermodynamic calculations, *Nature*, *375*, 308–311.
- Behr, Y., J. Townend, S. Bannister, and M. K. Savage (2010), Shear velocity structure of the Northland Peninsula, New Zealand, inferred from ambient noise correlations, *J. Geophys. Res.*, *115*, B05309, doi:10.1029/2009JB006737.
- Berryman, J. G. (1995), Mixture theories for rock properties, in *American Geophysical Union Handbook of Physical Constants*, edited by T. J. Ahrens, pp. 205–228, AGU, Washington, D. C.
- Berryman, J. G., and E. A. Berge (1993), Rock elastic properties: Dependence on microstructure, in *Homogenization and Constitutive Modeling for Heterogeneous Materials*, in *Proceedings of the Symposium on Homogenization and Constitutive Modeling for Heterogeneous Materials*, University of Virginia, Charlottesville, Virginia, June 6–9, 1993, edited by C. S. Chang and J. W. Ju, pp. 1–13, ASME, New York.

- Blundy, J. D., T. J. Falloon, B. J. Wood, and J. A. Dalton (1995), Sodium partitioning between clinopyroxene and silicate melts, *J. Geophys. Res.*, *100*, 15,501–15,516, doi:10.1029/95JB00954.
- Blundy, J. D., J. A. C. Robinson, and B. J. Wood (1998), Heavy REE are compatible in clinopyroxene on the spinel lherzolite solidus, *Earth Planet. Sci. Lett.*, *160*, 493–504.
- Bockris, J. O. M., J. A. Kitchener, S. Ignatowicz, and J. W. Tomlinson (1952), Electric conductance in liquid silicates, *Trans. Faraday Soc.*, *48*, 75–91.
- Bonatti, E., M. Ligi, D. Brunelli, A. Cipriani, P. Fabretti, V. Ferrante, L. Gasperini, and L. Ottolini (2003), Mantle thermal pulses below the Mid-Atlantic Ridge and temporal variations in the formation of oceanic lithosphere, *Nature*, *423*, 499–505.
- Boucher, S. (1976), Modules effectifs de matériaux composites quasi homogènes et quasi isotropes, constitués d'une matrice élastique et d'inclusions élastiques. II Cas des concentrations finies en inclusions, *Rev. Metall.*, *22*, 31–36.
- Caricchi, L., F. Gaillard, J. Mecklenburg, and E. Le Trong (2011), Experimental determination of electrical conductivity during deformation of melt-bearing olivine aggregates: Implications for electrical anisotropy in the oceanic low velocity zone, *Earth Planet. Sci. Lett.*, *302*, 81–94.
- Constable, S., and G. Heinson (2004), Hawaiian hot-spot swell structure from seafloor MT sounding, *Tectonophysics*, *389*, 111–124.
- Constable, S. (2006), SEO3: A new model of olivine electrical conductivity, *Geophys. J. Int.*, *166*, 435–437.
- Dai, L., and S.-I. Karato (2009), Electrical conductivity of orthopyroxene: Implications for the water content of the asthenosphere, *Proc. Jpn. Acad. Ser. B*, *85*, 466–475.
- Delorey, A. A., R. A. Dunn, and J. B. Gaherty (2005), Surface wave tomography of the upper mantle beneath the Reykjanes Ridge with implications for ridge-hot spot interaction, *J. Geophys. Res.*, *112*, B08313, doi:10.1029/2006JB004785.
- Desissa, M., N. E. Johnson, K. A. Whaler, S. Hautot, S. Fisseha, and G. J. K. Dawes (2013), A mantle magma reservoir beneath an incipient mid-ocean ridge in Afar, Ethiopia, *Nat. Geosci.*, *6*, 861–865, doi:10.1038/NGEO1925.
- Draper, D. S. (1992), Spinel lherzolite xenoliths from Lorena Butte, Simcoe mountains, southern Washington (USA), *J. Geol.*, *100*, 766–776.
- Duffy, J. A., and M. D. Ingram (1976), An interpretation of glass chemistry in terms of the Optical Basicity concept, *J. Non-Cryst. Solids*, *21*, 373–410.
- Duffy, T. S., and D. L. Anderson (1989), Seismic velocities in mantle minerals and the mineralogy of the upper mantle, *J. Geophys. Res.*, *94*(B2), 1895–1912, doi:10.1029/JB094iB02p01895.
- Dunn, R. A., and D. W. Forsyth (2003), Imaging the transition between the region of mantle melt generation and the crustal magma chamber beneath the southern East Pacific Rise with short-period Love waves, *J. Geophys. Res.*, *108*(B7), 2352, doi:10.1029/2002JB002217.
- Evans, R. L., et al. (1999), Asymmetric electrical structure in the mantle beneath the East Pacific Rise at 17°S, *Science*, *286*, 752–756.
- Falloon, T. J., D. H. Green, L. V. Danyushevsky, and A. W. McNeill (2008), The composition of near-solidus partial melts of fertile peridotite at 1 and 1.5 GPa: Implications for the petrogenesis of MORB, *J. Petrol.*, *49*(4), 591–613.
- Faul, U. H., J. D. Fitz, and I. Jackson (2004), Shear wave attenuation and dispersion in melt-bearing olivine polycrystals: 2. Microstructural interpretation and seismological implications, *J. Geophys. Res.*, *109*, B06202, doi:10.1029/2003JB002407.
- Gaillard, F. (2004), Laboratory measurements of electrical conductivity of hydrous and dry silicic melts under pressure, *Earth Planet. Sci. Lett.*, *218*(1–2), 215–228, doi:10.1016/S0012-821X(03)00639-3.
- Gaillard, F., and G. Iacono Marziano (2005), Electrical conductivity of magma in the course of crystallization controlled by their residual liquid composition, *J. Geophys. Res.*, *110*, B06204, doi:10.1029/2004JB003282.
- Gassmann, F. (1951), Über die elastizität poröser medien, *Viertel-jahrsschr. Naturforsch. Ges.*, *96*, 1–23.
- Ghiorso, M. S., M. M. Hirschmann, P. W. Reiners, and V. C. Kress III (2002), The pMELTS: A revision of MELTS for improved calculation of phase relations and major element partitioning related to partial melting of the mantle to 3 GPa, *Geochem. Geophys. Geosyst.*, *3*(5), doi:10.1029/2001GC000217.
- Grant, F. S., and G. F. West (1965), *Interpretation Theory in Applied Geophysics*, 583 pp., McGraw-Hill Book Co., New York.
- Hammond, W. C., and E. D. Humphreys (2000a), Upper mantle seismic wave velocity: Effects of realistic partial melt geometries, *J. Geophys. Res.*, *105*(B5), 10,975–10,986, doi:10.1029/2000JB900041.
- Hammond, W. C., and E. D. Humphreys (2000b), Upper mantle seismic wave velocity: Effects of realistic partial melt distribution, *J. Geophys. Res.*, *105*(B5), 10,987–10,999, doi:10.1029/2000JB900042.
- Hashin, Z., and S. Shtrikman (1962), A variational approach to the theory of the effective magnetic permeability of multiphase materials, *J. Appl. Phys.*, *33*, 3125–3131.
- Heise, W., T. G. Caldwell, H. M. Bibby, and S. L. Bennie (2010), Three-dimensional electrical resistivity image of magma beneath an active continental rift, Taupo Volcanic Zone, New Zealand, *Geophys. Res. Lett.*, *37*, L10301, doi:10.1029/2010GL043110.
- Hirose, K., and I. Kushiro (1993), Partial melting of dry peridotites at high pressures: Determination of compositions of melts segregated from peridotite using aggregates of diamond, *Earth Planet. Sci. Lett.*, *114*, 477–489.
- Hirschmann, M. M., M. S. Ghiorso, L. E. Waslylenki, P. D. Asimow, and E. M. Stolper (1998), Calculation of peridotite partial melting from thermodynamic models of minerals and melts. I. Review of methods and comparison with experiments, *J. Petrol.*, *39*(6), 1091–1115.
- Hirschmann, M. M., M. S. Ghiorso, and E. M. Stolper (1999), Calculation of peridotite partial melting from thermodynamic models of minerals and melts. II. Isobaric variations in melts near the solidus and owing to variable source composition, *J. Petrol.*, *40*(2), 297–313.
- Karato, S. (1993), Importance of anelasticity in the interpretation of seismic tomography, *Geophys. Res. Lett.*, *20*, 1623–1626, doi:10.1029/93GL01767.
- Kawahara, M., Y. Ozima, K. Morinaga, and T. Yanagase (1978), The electrical conductivity of Na₂O-SiO₂-MgO and CaO-SiO₂-MgO melts, *J. Jpn. Inst. Metals*, *42*, 618–623.
- Kawakatsu, H., P. Kumar, Y. Takei, M. Shinohara, T. Kanazawa, E. Araki, and K. Suyehiro (2009), Seismic evidence for sharp lithosphere-asthenosphere boundaries of oceanic plates, *Science*, *324*, 499–502.
- Kelbert, A., G. D. Egbert, and C. deGroot-Hedlin (2011), Crust and upper mantle electrical conductivity beneath the Yellowstone hotspot track, *Geology*, *40*, 447–450, doi:10.1130/G32655.
- Kelbert, A., G. Egbert, and C. deGroot-Hedlin (2012), Crust and upper mantle electrical conductivity beneath the Yellowstone Hotspot Track, *Geology*, *40*(5), 447–450.
- Kelley, K. A., T. Plank, S. Newman, E. M. Stolper, T. L. Grove, S. Parman, and E. H. Hauri (2010), Mantle melting as a function of water content beneath the Mariana Arc, *J. Petrol.*, *51*(8), 1711–1738.
- Key, K., S. Constable, L. Liu, and A. Pommier (2013), Electrical image of passive mantle upwelling beneath the northern East Pacific Rise, *Nature*, *495*, doi:10.1038/nature11932.
- Klein, E. M., and C. H. Langmuir (1987), Global correlations of ocean ridge basalt chemistry with axial depth and crustal thickness, *J. Geophys. Res.*, *92*(B8), 8089–8115, doi:10.1029/JB092iB08p08089.
- Kohlstedt, D. L. (1992), Structure, rheology and permeability of partially molten rocks at low melt fractions, in *Mantle Flow and Melt Generation at Mid-Ocean Ridges*, edited by J. Phipps Morgan, D. K. Blackman, and J. M. Sinton, pp. 103–121, AGU, Washington, D. C.

- Laske, G., A. Markee, J. A. Orcutt, C. J. Wolfe, J. A. Collins, S. C. Solomon, R. S. Detrick, D. Bercovici, and E. H. Hauri (2011), Asymmetric shallow mantle structure beneath the Hawaiian Swell—Evidence from Rayleigh waves recorded by the PLUME network, *Geophys. J. Int.*, *187*, 1725–1742.
- Li, H., and M. Tomozawa (1996), Effects of water in simulated borosilicate-based nuclear waste glasses on their properties, *J. Non-Cryst. Solids*, *195*, 188–198.
- Mainprice, D. (1997), Modelling the anisotropic seismic properties of partially molten rocks found at mid-ocean ridges, *Tectonophysics*, *279*, 161–179.
- Mathieu, R., G. Libourel, E. Deloule, L. Tissandier, C. Rapin, and R. Podor (2011), Na₂O solubility in CaO-MgO-SiO₂ melts, *Geochim. Cosmochim. Acta*, *75*, 608–628.
- Matsuno, T., R. L. Evans, N. Seama, and A. D. Chave (2012), Electromagnetic constraints on a melt region beneath the central Mariana back-arc spreading ridge, *Geochem. Geophys. Geosyst.*, *13*, Q10017, doi:10.1029/2012GC004326.
- Maumus, J., N. Bagdassarov, and H. Schmeling (2005), Electrical conductivity and partial melting of mafic rocks under pressure, *Geochim. Cosmochim. Acta*, *69*(19), 4703–4718, doi:10.1016/j.gca.2005.05.010.
- McGregor, L. M., S. Constable, and M. C. Sinha (1998), The RAMESSES experiment—III. Controlled-source electromagnetic sounding of the Reykjanes Ridge at 57°45'N, *Geophys. J. Int.*, *135*, 773–789.
- McKenzie, D. (1984), The generation and compaction of partially molten rock, *J. Petrol.*, *25*, 713–765.
- McKenzie, D., and M. J. Bickle (1988), The volume and composition of melt generated by extension of the lithosphere, *J. Petrol.*, *29*(3), 625–679.
- Moretti, R. (2005), Polymerisation, basicity, oxidation state and their role in ionic modeling of silicate melts, *Ann. Geophys.*, *48*, 583–608.
- Naif, S., K. Key, S. Constable, and R. L. Evans (2013), Melt-rich channel observed at the lithosphere-asthenosphere boundary, *Nature*, doi:10.1038/nature11939.
- Ni, H., H. Keppler, and H. Behrens (2011a), Electrical conductivity of hydrous basaltic melts: Implications for partial melting in the upper mantle, *Contrib. Mineral. Petrol.*, *162*, 637–650.
- Ni, H., H. Keppler, M. A. G. M. Manthilake, and T. Katsura (2011b), Electrical conductivity of dry and hydrous NaAlSi₃O₈ glasses and liquids at high pressures, *Contrib. Mineral. Petrol.*, *162*, 501–s, doi:10.1007/s00410-011-0608-5.
- Niu, Y. (1997), Mantle melting and melt extraction processes beneath ocean ridges: Evidence from abyssal peridotites, *J. Petrol.*, *38*(8), 1047–1074.
- Noritake, F., K. Kawamura, T. Yoshino, and E. Takahashi (2012), Molecular dynamics simulation and electrical conductivity measurement of Na₂O·3SiO₂ melt under high pressure; relationship between its structure and properties, *J. Non-Cryst. Solids*, *358*, 3109–3118.
- Partzsch, G. M., F. R. Schilling, and J. Arndt (2000), The influence of partial melting on the electrical behavior of crustal rocks: Laboratory examinations, model calculations and geological interpretations, *Tectonophysics*, *317*, 189–203.
- Pommier, A., F. Gaillard, M. Pichavant, and B. Scaillet (2008), Laboratory measurements of electrical conductivities of hydrous and dry Mount Vesuvius melts under pressure, *J. Geophys. Res.*, *113*, B05205, doi:10.1029/2007JB005269.
- Pommier, A. (2013), Interpretation of magnetotelluric results using laboratory measurements, *Surv. Geophys.*, doi:10.1007/s10712-013-9226-2.
- Pommier, A., R. L. Evans, K. Key, J. A. Tyburczy, S. Mackwell, and J. Elsenbeck (2013), Prediction of silicate melt viscosity from electrical conductivity: A model and its geophysical implications, *Geochem. Geophys. Geosyst.*, *14*, 1685–1692, doi:10.1002/2012GC004467.
- Pommier, A., F. Gaillard, M. Malki, and M. Pichavant (2010), Methodological re-evaluation of the electrical conductivity of silicate melts, *Am. Mineral.*, *95*, 284–291.
- Pozgay, S. H., D. A. Wiens, J. A. Conder, H. Shiobara, and H. Sugioka (2009), Seismic attenuation tomography of the Mariana subduction system: Implications for thermal structure, volatile distribution, and slow spreading dynamics, *Geochem. Geophys. Geosyst.*, *10*, Q04X05, doi:10.1029/2008GC002313.
- Presnall, D. C., C. L. Simmons, and H. Porath (1972), Changes in electrical conductivity of a synthetic basalt during melting, *J. Geophys. Res.*, *77*, 5665–5672, doi:10.1029/JB077i029p05665.
- Rai, C. S., and M. H. Manghni (1977), Electrical conductivity of basalts to 1550 °C, in *Magma Genesis: Bulletin 96*, edited by H. J. B. Dick, pp. 219–232, Oregon Department of Geology and Mineral Industries, Portland.
- Roberts, J. J., and J. A. Tyburczy (1999), Partial-melt electrical conductivity: Influence of melt composition, *J. Geophys. Res.*, *104*, 7055–7065, doi:10.1029/1998JB900111.
- Robinson, J. A. C., B. J. Wood, and J. D. Blundy (1998), The beginning of melting of fertile and depleted peridotite at 1.5 GPa, *Earth Planet. Sci. Lett.*, *155*, 97–111.
- Schiano, P., and R. Clocchiatti (1994), Worldwide occurrence of silica-rich melts in subcontinental and suboceanic mantle minerals, *Nature*, *368*, 621–624.
- Schilling, F. R., G. M. Partzsch, H. Brasse, and G. Schwarz (1997), Partial melting below the magmatic arc in the central Andes deduced from geoelectromagnetic field experiments and laboratory data, *Phys. Earth Planet. Int.*, *103*, 17–31.
- Schmeling, H. (1985), Numerical models on the influence of partial melt on elastic, anelastic and electric properties of rocks. Part I: Elasticity and anelasticity, *Phys. Earth Planet. Int.*, *41*, 34–57.
- Schmeling, H. (1986), Numerical models on the influence of partial melt on elastic, anelastic and electric properties of rocks. Part II: Electrical conductivity, *Phys. Earth Planet. Int.*, *43*, 123–136.
- Shankland, T. J., and A. Duba (1990), Standard electrical conductivity of isotropic, homogeneous olivine in the temperature range 1200–1500 °C, *Geophys. J. Int.*, *103*, 25–31.
- Simonnet, C., J. Phalippou, and M. Malki (2003), Electrical conductivity measurements of oxides from molten state to glassy state, *Rev. Sci. Instrum.*, *74*, 2805–2810.
- Sinha, M. C., S. C. Constable, C. Pierce, A. White, G. Heinson, L. M. MacGregor, and D. A. Navin (1998), Magmatic processes at slow spreading ridges: Implications of the RAMESSES experiment at 57°45'N on the Mid-Atlantic Ridge, *Geophys. J. Int.*, *135*, 731–745.
- Sinton, J. M., and R. S. Detrick (1992), Mid-ocean ridge magma chambers, *J. Geophys. Res.*, *97*, 197–216, doi:10.1029/91JB02508.
- Smith, R. B., M. Jordan, B. Steinberger, C. M. Puskas, J. Farrell, G. P. Waite, S. Husen, W.-L. Chang, and R. O'Connell (2009), Geodynamics of the Yellowstone hotspot and mantle plume: Seismic and GPS imaging, kinematics, and mantle flow, *J. Volcanol. Geotherm. Res.*, *188*, 26–56.
- Stacey, F. D. (1992), *Physics of the Earth*, 3rd ed., 513 pp., Brookfield Press, Australia.
- Stork, A. L., G. W. Stuart, C. M. Henderson, D. Keir, and J. O. S. Hammond (2013), Uppermost mantle (P_n) velocity model for the Afar region, Ethiopia: An insight into rifting processes, *Geophys. J. Int.*, *193*, 321–328.
- Stratford, W. R., and T. A. Stern (2006), Crust and upper mantle structure of a continental backarc: Central North Island, New Zealand, *Geophys. J. Int.*, *166*, 469–484.

- Takahashi, E., and I. Kushiro (1983), Melting of a dry peridotite at high-pressures and basalt magma genesis, *Am. Mineral.*, *68*, 859–879.
- Takei, Y. (2000), Acoustic properties of partially molten media studied on a simple binary system with a controllable dihedral angle, *J. Geophys. Res.*, *105*(B7), 16,665–16,682, doi:10.1029/2000JB900124.
- ten Grotenhuis, S. M., M. R. Drury, C. J. Spiers, and C. J. Peach (2005), Melt distribution in olivine rocks based on electrical conductivity measurements, *J. Geophys. Res.*, *110*, B12201, doi:10.1029/2004JB003462.
- Toomey, D. R., D. Joussetin, R. A. Dunn, W. S. D. Wilcock, and R. S. Detrick (2007), Skew of mantle upwelling beneath the East Pacific Rise governs segmentation, *Nature*, *446*, doi:10.1038/nature05679.
- Toomey, D. R., W. S. D. Wilcock, S. S. Solomon, W. C. Hammond, and J. A. Orcutt (1998), Mantle seismic structure beneath the MELT region of the East Pacific Rise from P and S wave tomography, *Science*, *280*, 1224–1227.
- Tyburczy, J. A., and H. S. Waff (1983), Electrical conductivity of molten basalt and andesite to 25 kilobars pressure: Geophysical significance and implications for charge transport and melt structure, *J. Geophys. Res.*, *88*(B3), 2413–2430, doi:10.1029/JB088iB03p02413.
- Tyburczy, J. A., and H. S. Waff (1985), High-pressure electrical conductivity in naturally occurring silicate liquids, in *Point Defects in Minerals, Geophys. Monogr. Ser.*, vol. 31, edited by R. N. Schock, pp. 78–87, AGU, Washington, D. C.
- Waff, H. S. (1974), Theoretical considerations of electrical conductivity in a partially molten mantle and implications for geothermometry, *J. Geophys. Res.*, *79*, 4003–4010, doi:10.1029/JB079i026p04003.
- Waff, H. S., and D. F. Weill (1975), Electrical conductivity of magmatic liquids: Effects of temperature, oxygen fugacity and composition, *Earth Planet. Sci. Lett.*, *28*, 254–260.
- Wagner, L., D. W. Forsyth, M. J. Fouch, and D. E. James (2010), Detailed three-dimensional shear wave velocity structure of the northwestern United States from Rayleigh wave tomography, *Earth Planet. Sci. Lett.*, *299*, 273–284.
- Walter, M. J., and D. C. Presnall (1994), Melting behavior of simplified lherzolite in the system CaO-MgO-Al₂O₃-SiO₂-Na₂O from 7 to 35 kbar, *J. Petrol.*, *35*(2), 329–359.
- Wasylenki, L. E., M. B. Baker, M. M. Hirschmann, and E. M. Stolper (1996), The effect of source depletion on equilibrium mantle melting, *EOS Trans.*, *77*, 847.
- Wasylenki, L. E., M. B. Baker, A. J. R. Kent, and E. M. Stolper (2003), Near-solidus melting of the shallow upper mantle: Partial melting experiments on depleted peridotite, *J. Petrol.*, *44*(7), 1163–1191.
- Watt, J. P., G. F. Davies, and R. J. O'Connell (1976), The elastic properties of composite materials, *Rev. Geophys. Space Phys.*, *14*(4), 541–563.
- Williams, Q., and E. J. Garnero (1996), Seismic evidence for partial melt at the base of the Earth's mantle, *Science*, *273*, 1528–1530.
- Yang, X., H. Keppler, C. McCammon, H. Ni, Q. Xia, and Q. Fan (2011), The effect of water on the electrical conductivity of lower crustal clinopyroxene, *J. Geophys. Res.*, *116*, B04208, doi:10.1029/2010JB008010.